Article

Parameters of Collision and Adhesion Process Between a Rising Bubble and Quartz in Long-Chain Amine Solution and Their Correlation with Flotation

Shuling Gao [1],*, Bochao Li [1], Lifeng Ma [2], Wenbao Liu [1], Sikai Zhao [1] and Yanbai Shen [1]

1   School of Resources and Civil Engineering, Northeastern University, Shenyang 110819, China;
    2490134@stu.neu.edu.cn (B.L.); liuwenbao@mail.neu.edu.cn (W.L.); zhaosikai@mail.neu.edu.cn (S.Z.);
    shenyanbai@mail.neu.edu.cn (Y.S.)
2   BGRIMM Technology Group, Beijing 100160, China; malifeng@bgrimm.com
*   Correspondence: gaoshuling@mail.neu.edu.cn

Abstract: The successful adhesion of air bubbles to mineral particles is the crucial to flotation technology. This paper systematically investigates the parameters variation in the dynamic interaction process between a rising bubble and a quartz plate in long-chain amine solutions (dodecylamine, tedecylamine, and octadecylamine). The results show that the type and concentration of long-chain amine affected the collision and adhesion process between bubbles and quartz plates remarkably. The maximum rebound distance (rebound distance after the first collision) of bubbles and the stable-state liquid film thickness gradually decreases with the increase of reagent concentration. Additionally, the collision-rebound duration and induction time shorten accordingly, the surface tension of the solution decreases, the surface hydrophobicity of quartz increases, and the deformation degree and average movement velocity of bubbles decrease. With the increase in carbon chain length, the adsorption form of the amine collector and quartz surface becomes closer to vertical, and the density of water molecules decreases. The recovery of quartz particles is highest with octadecylamine systems, corresponding well with the changing trend in steady-state liquid film thickness. This research provides an effective method for in-depth analysis of the microscopic interaction mechanism between bubbles and mineral surfaces and the prediction of flotation results.

Keywords: flotation; bubble behavior; collision and adhesion; induction time; liquid film thickness

1. Introduction

Mineral resources are non-renewable. With the decrease in rich deposits and the increasing prevalence of poor, fine, and miscellaneous ores, the mineral processing field will face the problem of fine particle separation for a long time. As an effective method of fine particle separation, flotation is widely used in the processing field of nonferrous metal ores, iron ores, non-metallic ores, coal, and other resources, and its status is pivotal and irreplaceable in many cases. The generation of bubbles is the basic premise of flotation. The size, distribution, and movement characteristics of bubbles, as well as the collision, adhesion, and formation of a stable mineralized froth layer between the bubbles and particles, directly impact the flotation effect [1–5]. Therefore, research on bubbles and the interaction between bubbles and particles has long attracted considerable attention. With advancements in the diversification and precision of detection methods, research perspectives have become more diversified and unique.

At present, research methods on the interaction process between bubbles and particles and their influencing factors mainly fall into two directions: thermodynamics and dynamics. Thermodynamics determines the trend of bubble mineralization by calculating the energy changes before and after, while dynamics divides the interaction process between bubbles and quartz into three sub-processes: collision, adhesion, and desorption [6,7].

In thermodynamic studies, it is generally assumed that bubbles do not deform before and after contact with the particles, and the residual hydration film is not considered. The change of free energy before and after adhesion is calculated. It is believed that, except for completely hydrophilic particles (contact angle is zero), the adhesion between bubbles and particles is spontaneous (free energy is less than zero). The higher the hydrophobicity of ore particles, the larger the contact angle and the stronger the spontaneous tendency. The thermodynamic study of gas–solid interactions is based on the interface wetting contact angle theory. It assumes that a liquid droplet on a solid surface, does not develop fully but forms an angle with the solid surface. The tangent line of the gas–liquid interface is used at the intersection of the three phases—solid, liquid, and gas. The angle between the tangent line and the boundary of the solid liquid is the contact angle, which is represented by θ [8–11]. It is worth pointing out that bubble mineralization takes 10 min or longer to reach the equilibrium contact angle. In the flotation process, the time of bubble and particle collision contact is only 5–8 ms, so it is impossible to achieve equilibrium. In addition, hydration film has an energy barrier; it is unrealistic not to consider the change of free energy in hydration film, so some thermodynamic inferences should be treated with caution.

Flotation kinetics divides the flotation process into three independent sub-processes: collision, adhesion, and desorption. First, bubbles and mineral particles collide with each other in the slurry. Then the liquid film on the surface of the bubbles thins, forming a gas-liquid-solid three-phase wetting perimeter on the surface of the particles. As the three-phase wetting perimeter expands, and the bubbles and mineral particles can adhere successfully. Some of the bubble-particle polymers do not desorb due to external forces during the ascent and eventually float up into the foam layer to become a concentrate. However, some mineral particles separate from the bubbles under the action of external forces [12,13]. Therefore, the probability of mineral flotation can be described by three independent processes: collision probability, adhesion probability, and desorption probability [14,15].

In recent years, the precise development of high-speed photography technology has provided an effective means for gaining an in-depth understanding of the characteristics and behavior of bubbles in flotation pulp. How to select appropriate equipment parameters and operating conditions to make bubbles reach the most favorable state for mineralization will be a focus of future flotation test research and production process control. Most research on the interaction between bubbles and particles uses unique observation devices either to fix bubbles and allow particles collide with them or fix minerals at the top and produce bubbles to collide with them from below. A high-speed camera is used to record the collision process in each setup The former is used to measure sliding contact time. The latter is suitable for determining collision contact time [16–19]. Using high-speed camera technology, researchers have explored the movement state and size distribution of bubbles under different conditions, as well as differences in time parameters such as liquid film drainage, three-phase wetting perimeter formation, diffusion time, and induction time during the particle collision and their impact on the flotation effect. It has been recognized that to capture particles and bubbles effectively, they must undergo a near-collision process controlled by fluid dynamics. The particles and bubbles are first brought within the gravitational range, and then the liquid film between them expels the liquid. This indicates that liquid film thickness is critical for capture to occur. The liquid–gas interface then retracts to the surface of the solid particle until a stable wetting perimeter is established. After this attachment process, the particles and bubbles combine [20–23].

However, most studies on the characteristics of bubbles and the collision process with particles have used specific surfactants and planes of unique materials instead of hydrophilic and hydrophobic minerals, respectively. However, in the actual flotation process, the conditions of flotation reagents are complicated, and the interaction between reagents may also affect the bubble characteristics [24]. In the actual flotation process, the surface properties of particles are realized through the adsorption of reagents, and the flow field environment also has a non-negligible impact on the characteristics of bubbles and the

interaction process with minerals. Therefore, although these studies have gained a deeper understanding of the interaction process between particles and bubbles, they are limited in guiding the production practice.

The adhesion of particles on the bubble surface is closely related to the chemical and physicochemical properties of particles and the bubble surface [25–27]. Not all particles that collide with the bubble can adhere to the bubble's surface; of those that are capable, only a portion successfully adhere. Although high-speed camera technology can directly observe the changing process of each stage, it cannot provide information on the force. In recent years, the continuous improvement of atomic force microscope (AFM) functionality has provided conditions for studying the force between bubbles and mineral particles from a microscopic perspective [28–31]. Naoyuki Ishida [32] measured the force between spherical silica particles and bubbles in a dodecylamine chloride (DAH) aqueous solution using an atomic force microscope. The test found that in a surfactant solution, the electrostatic repulsion force could be observed at a considerable distance between particles and bubbles and became attractive as the distance approached. The range of gravitational action increased with the increase in DAH concentration. Quantitative analysis data obtained by AFM can further clarify the interaction mechanism between bubbles and mineral particles under different solution conditions. Zhu Chunyun et al. [33] conducted a test using AFM bubble probe technology to analyze the adhesion mechanism between bubbles and different hydrophobic coal surfaces at micro and nano scales. The results show that for strong hydrophobic coal surface surfaces, hydrophobic force can overcome surface repulsion and induce bubble adhesion, while fluid force can hinder or even inhibit bubble adhesion. Hydrophobic power is insufficient for medium and weak hydrophobic coal surfaces to overcome repulsive surface force. In contrast, fluid force can increase the attraction between bubbles and coal surfaces, thus increasing the adhesion probability. Zhang Fanfan et al. [34] used AFM to test the interaction force between particles and bubbles. They obtained information on the interaction force by recording the microcantilever deformation during the insertion and removal of the probe needle. The results show that the thickness of the broken liquid film is 114.34 nm when a micron-sized bubble is attached to the hydrophobic particles, which is about two orders of magnitude different from the thickness of the broken liquid film between the millimeter bubble and the particles. This indicates that the thickness of the broken liquid film is related to the bubble size when bubbles attach to particles. The hydrophobic interaction between particle bubbles was investigated using AFM and DWFA by Xing Yaowen et al. [35]. Four different positions were selected in the experiments to ensure the accuracy of the results, and the results showed that hydrophobic particles undergo a jump-in phenomenon between the occurrence of adhesion and the maximum adhesion distance of 20–40 nm. Israelachvili et al. [36] investigated the hydrophobic coal particles–stearic acid system using the AFM technique. They detected a repulsive force at a distance of about 75 nm, which increased as the distance decreases. This repulsive force may be due to electrostatic repulsion between the carboxyl groups in stearic acid molecules and the negatively charged coal surface, while the attractive force may be due to the hydrophobic gravitational force between the hydrocarbon chains in the stearic acid and the hydrophobic coal surface.

This paper studied the dynamic process of rising bubbles with a certain speed approaching the quartz surface, colliding, bouncing, and finally adhering to the flotation solution of long-chain amines using a high-speed dynamic camera. The curve of the vertex position on the bubble with time, the collision and rebound time between the bubble and quartz, the maximum rebound distance, the induction time, and the thickness of the liquid film in the stable state (the thickness of the residual liquid after the bubble and the quartz surface are stably attached) were investigated with the type and amount of long-chain amine. At the same time, the changing characteristics of the rising bubble rate, solution surface tension, quartz surface contact angle, and adsorption parameters of chemical molecules and quartz, as influenced by changes in reagent molecules and concentration, were also investigated. The correlation between the interaction parameters of bubbles and

particles and the flotation results was further established based on the results of the quartz flotation test.
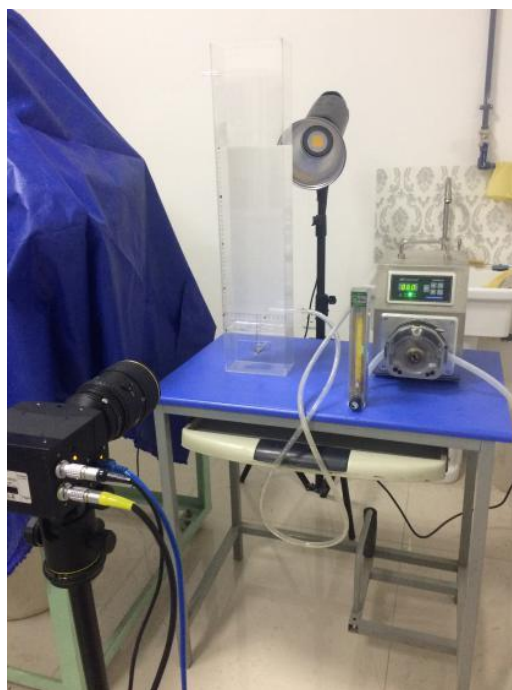
2. Materials and Methods

2.1. High-Speed Dynamic Camera System and Data Treating

Figures 1 and 2 show the observation system diagram and a picture of the real product of the interaction between the bubble and the quartz plate.
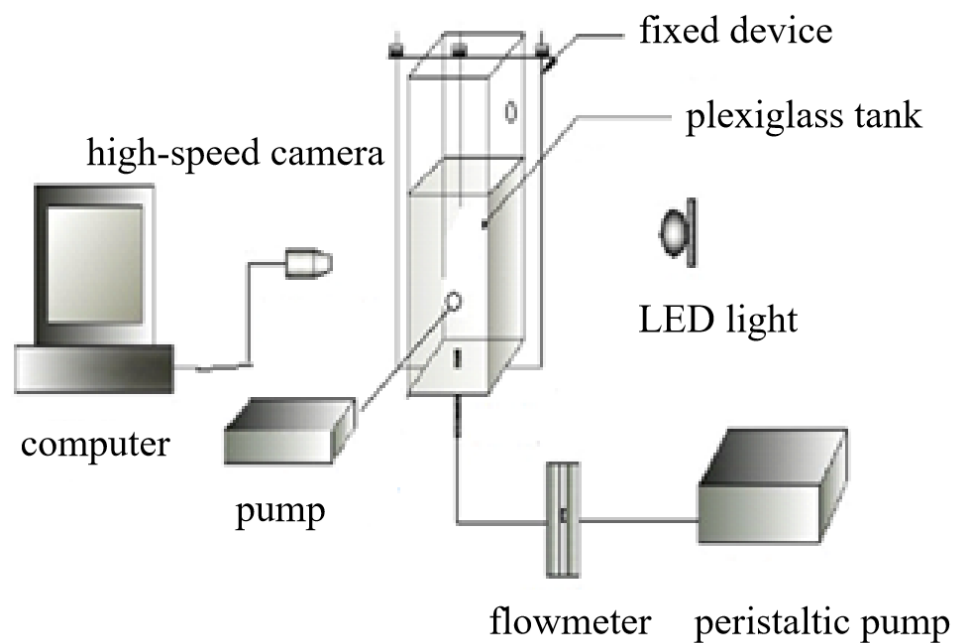
Figure 1. Schematic illustration of the interaction between a bubble and quartz in the observation system.

Figure 2. Physical drawing of the interaction between a bubble and quartz plate in the observation system.

The observation system comprises a high-speed dynamic camera (OLYMPUS I-SPEED221), homemade plexiglass trough, LED lamp, peristaltic pump, and computer. The observation device for interactions between bubbles and quartz plates is a homemade plexiglass tank of 15 cm in length, 8 cm in breadth, and 60 cm in height. The plexiglass tube at the bottom of the side is connected to the pump and flowmeter to generate uniform bubbles for the system. In addition, the bottom and upper parts of the tank have external drainage pipes. The bottom, through the peristaltic pump water supply, adjusts the pump's power and changes the flow speed in the tank, allowing it to also be used to study the interaction process of bubbles and minerals in a dynamic environment. Through this research methodology and approach, we examined the rise of bubbles in water and amine collector solutions and their collision and adhesion with quartz surfaces. Bubble morphology and movement characteristics were also investigated.

The quartz samples used in the test were taken from the Qidashan Iron Ore concentrator produced by Angang Group. First, samples were crushed to −2 mm with a jaw crusher and roll crusher and then ground to −0.1 mm with a ceramic ball mill. After dewatering, the ground products were soaked three times in a 5% hydrochloric acid solution using a liquid-solid ratio of 3:1. The products were soaked for 24 h each time, and finally washed with distilled water until neutral, resulting in the extraction of quartz single mineral. The result of elemental analyses of the samples is shown in Table 1, which shows that the sample is mainly quartz, the SiO_2 content is more than 99%, and the chemical purity is high. Further screening obtained more than 80% quartz particles of −0.074 mm for the prepared quartz sample, which is used for single-mineral flotation.

Table 1. Elemental analysis of quartz.

Sample Name	SiO_2 %	Al_2O_3 %	Fe %	Mg %	MgO %
1	99.5	0.33	<0.001	<0.001	---

The quartz plate of the bubble–quartz adhesion observation system is obtained by pressing the quartz particles after they are treated with the corresponding reagent conditions. By fixing the quartz plate on the upper part of the system, the bubbles generated at the bottom rise and come into contact with it. A high-speed dynamic camera is used to capture the collision and adhesion process between the bubbles and the surface of the quartz particles. The microscopic process of the collision between the surface of the particles and the bubbles, along with the liquid film drainage under the conditions of dodecylamine, tetradecylamine, and octadecylamine with different concentrations, is observed and analyzed. In the coordinate system of data processing, the vertical coordinate of the horizontal plane between the quartz plate and water is set to zero, and the direction of bubble rise is set to the positive direction of the Y-axis.

The video of the interaction between bubbles and quartz was imported into I-speed control software version 1.0, a high-speed camera data processing software that can convert the video into pictures. After verification with the ruler of the observation system, the position of the top of the bubble was recorded to determine the movement of the bubble and the distance between the bubble and the quartz plate. Bubble centroids are widely used to investigate their trajectories with high accuracy [37,38]. The research focused on the process of bubbles rising and coming into contact with the quartz surface. Since the apex of the bubble first contacts the quartz surface, receives a specific extrusion, and rebounds, changes in the induction time and film thickness cannot be observed by tracking bubble centroids. Therefore, the coordinate of the bubble apex was utilized to examine its movement trajectory. The Y-axis coordinate of the plane at the bottom of the quartz plate was set to zero, and the shot image is shown in Figure 3.
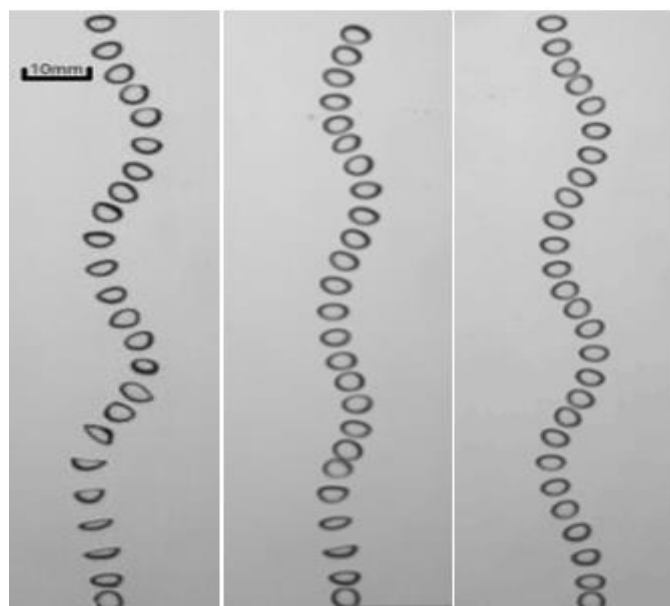
Figure 3. Motion path of a bubble.

The speed of the bubble is calculated according to the coordinates derived from the high-speed camera system. The bubble coordinates in the previous frame are taken as a reference. The displacement of the bubble in two adjacent frames is divided by the time interval, as shown in Equation (1):

$$v = (\sqrt{(x_i - x_{i-1})^2} + \sqrt{(y_i - y_{i-1})^2})/\Delta t \tag{1}$$

where (x_i, y_i) is the coordinate of the bubble at a particular moment and (x_{i-1}, y_{i-1}) is the coordinate of the bubble in the previous frame. Δt is the time interval—1.9 ms in this test—and the speed calculated by this method is the instantaneous speed of the bubble. The derived longitudinal position of the top of the bubble also characterizes the collision and adhesion process between the bubble and the quartz particles. In order to facilitate calculation, the Y-axis coordinate of the plane where the bottom of the quartz is located is set to zero, and the distance between the top of the bubble and the quartz plate after the rebound stops is the liquid film thickness between the two. In this experiment, two parameters—induction time and steady-state liquid film thickness—were used to quantitatively characterize the adhesion process between the bubble and the quartz surface. In order to improve the reliability of the data, 20 repeated shots were taken under each condition. Previous studies have shown that the liquid film thickness between bubbles and particles is related to the size of the bubbles and particles. Hence, this test's absolute value of liquid film thickness is still different from the actual flotation situation, which can be further improved based on this test.

*2.2. Contact Angle and Surface Tension Test*

A JC2000A contact angle measuring instrument measured the contact angle of the quartz particle surface under different reagent conditions. During the test, the treated quartz plate was placed on a platform, and the liquid drops were slowly dropped by turning the knob above the syringe. Using the picture of the droplet falling on the mineral surface, we used the five-point method to calculate the contact angle of the mineral surface.

The surface tension of dodecylamine, tetradecylamine, and octadecylamine solutions with different concentrations was measured using a JK99A automatic tensiometer. The test was conducted using the Wilhelmy method at about 20 ± 0.5 °C. Before measurement, solutions of different concentrations should be prepared, and 50 mL of the solution to be measured should be added to the glassware. Then, the surface tension should be measured.

The measurement of each concentration should be repeated at least three times, and the measurement results should be averaged. Using this research methodology and approach, the changes in the surface tension of the solution and the surface hydrophobicity of quartz were explored, respectively.

2.3. Molecular Dynamics Simulation

Structural characterization of dodecylamine, tetradecylamine, and octadecylamine collectors was carried out using Materials Studio 2020 software, as shown in Figure 4.
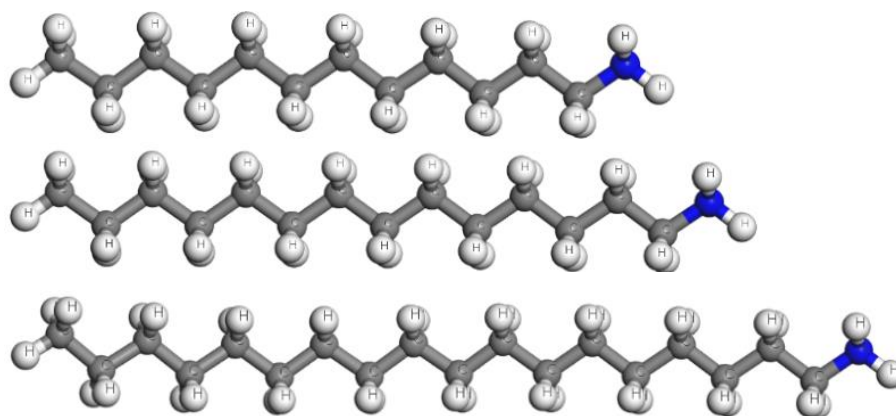
Figure 4. The molecular structure of amine collectors.

The hydrophobicity increases with increasing carbon chain length, and octadecylamine has the best hydrophobicity compared to the other two collectors. Nitrogen atoms in the amine collector molecule can accept protons to form cations (RNH_3+), which can be adsorbed by the electrostatic force of attraction with the negative charges on the quartz surface, thus changing the surface's hydrophobicity.

The molecular dynamics of three kinds of water-reagent-quartz (101) surface systems were simulated using Materials Studio 2020 software, and the adsorption energy, order degree, and oxygen atom density of the amine collectors and quartz were calculated, respectively. Using this simulation methodology and approach, the variation characteristics of the parameters of the adsorption process between reagent molecules and quartz were investigated.

Adsorption energy can be used to compare the adsorption strength between different reagents and minerals quantitatively. The calculation method for adsorption energy between reagents and quartz surface under a vacuum environment is as follows:

$$\Delta E_{ad} = E_{total} - (E_{collector} + E_{quartz}) \tag{2}$$

where ΔE_{ad} is the adsorption energy of the cationic collector interacting with the quartz (101) surface under vacuum conditions, E_{total} is the total energy of the system after the interaction of the quartz (101) surface with the cationic collector under vacuum conditions, $E_{collector}$ is the total energy of the cationic collector, and E_{quartz} is the total energy of the quartz (101) face. When the value of ΔE_{ad} is negative, it indicates that the reaction can be spontaneous. The larger the value of ΔE_{ad}, the easier the reaction is to proceed with and the more stable the adsorption. When the value of ΔE_{ad} is positive, the reaction is more difficult to proceed with.

In order to quantitatively compare the differences in the adsorption structures of dodecylamine, tetradecylamine, and octadecylamine ions on a quartz surface, the ordered parameter S, which is used to characterize the angle between the definition vector and the

reference vector, is used to characterize the adsorption morphology of the collector on the mineral surface. The calculation method is as follows:

$$S = \frac{1}{2}\left(3\,cos\theta^2 - 1\right)$$

(3)

where θ is the angle between the specified vector and the reference vector, that is, the angle between the definition vector b_i and the z-axis, which is the reference vector perpendicular to the surface of quartz (101) in the study system, and b_i is defined as the vector along the N-C skeleton, starting with the head nitrogen atom of the collector, and pointing to the i-th carbon atom on the ion chain. The ordered parameter S has a value between −0.5 and 1.0. When the value of the ordered parameter S is −0.5, the defined vector b_i is perpendicular to the z-axis of the reference vector. When the value of the ordered parameter S is 1.0, the vector b_i is defined parallel to the z-axis of the reference vector (in the same direction or the opposite direction). When the value of the ordered parameter S is 0.0, the orientation of the defined vector b_i concerning the z-axis of the reference vector is random.

The density of water molecules at different distances from the quartz surface is characterized by counting the density of the water oxygen atoms. The calculation method is as follows:

$$\rho_z = \frac{N(z - \Delta z/2, z + \Delta z/2) \times M}{\Delta z \times S}$$

(4)

where $N(z - \frac{\Delta z}{2}, z + \Delta z/2)$ is the average number of oxygen atoms in the interval $(z - \frac{\Delta z}{2}, z + \Delta z/2)$ (Δz = 0.01), M is the mass of oxygen atoms, and S is the area of the quartz base surface.

2.4. Flotation Test

The single mineral flotation test was carried out in the $XFGC_{II}$ hanging cell flotation machine with a volume of 35 mL. Each time, 5.0 g quartz particles were weighed, about 30 mL distilled water was added for pulping for 2 min, and then the collector was added and stirred for 2 min before flotation began. Because the amine collector has a comprehensive effect of foaming, adjusting the hydrophobicity of the solid surface, and reducing the surface tension, the frother is generally no longer added to the flotation pulp [39–41]. Collector species included dodecylamine, tetradecylamine, and octadecylamine at concentrations of 0.25 mol/L, 0.5 mol/L, 0.75 mol/L, and 1 mol/L, respectively. The flotation time was 4 min, and then the flotation products were dried and weighed to calculate the quartz recovery rate. Based on the results of the flotation tests, the recovery of quartz particles and the correlation with the parameters of the liquid drainage process were analyzed and explored, respectively.

3. Results and Discussion

3.1. The Rise of Bubbles in Water and Amine Collector Solutions and Their Collision and Adhesion with Quartz Surfaces

The bubbles' rising and contact collision process with the quartz surface was observed using an established high-speed dynamic camera system to obtain the bubbles' rising and behaviors of collision and adhesion with the quartz surface in water and amine collector solutions.

3.1.1. Time Curve of Vertex Position on Bubble

The collision and adhesion process between the bubble and the quartz surface is analyzed by recording the position change of the upper vertex in still water. The movement trajectory of bubbles in pure water and solutions of dodecylamine (DDA), tetradecylamine (TDA), and octadecylamine (ODA) at different concentrations is shown in Figure 5.
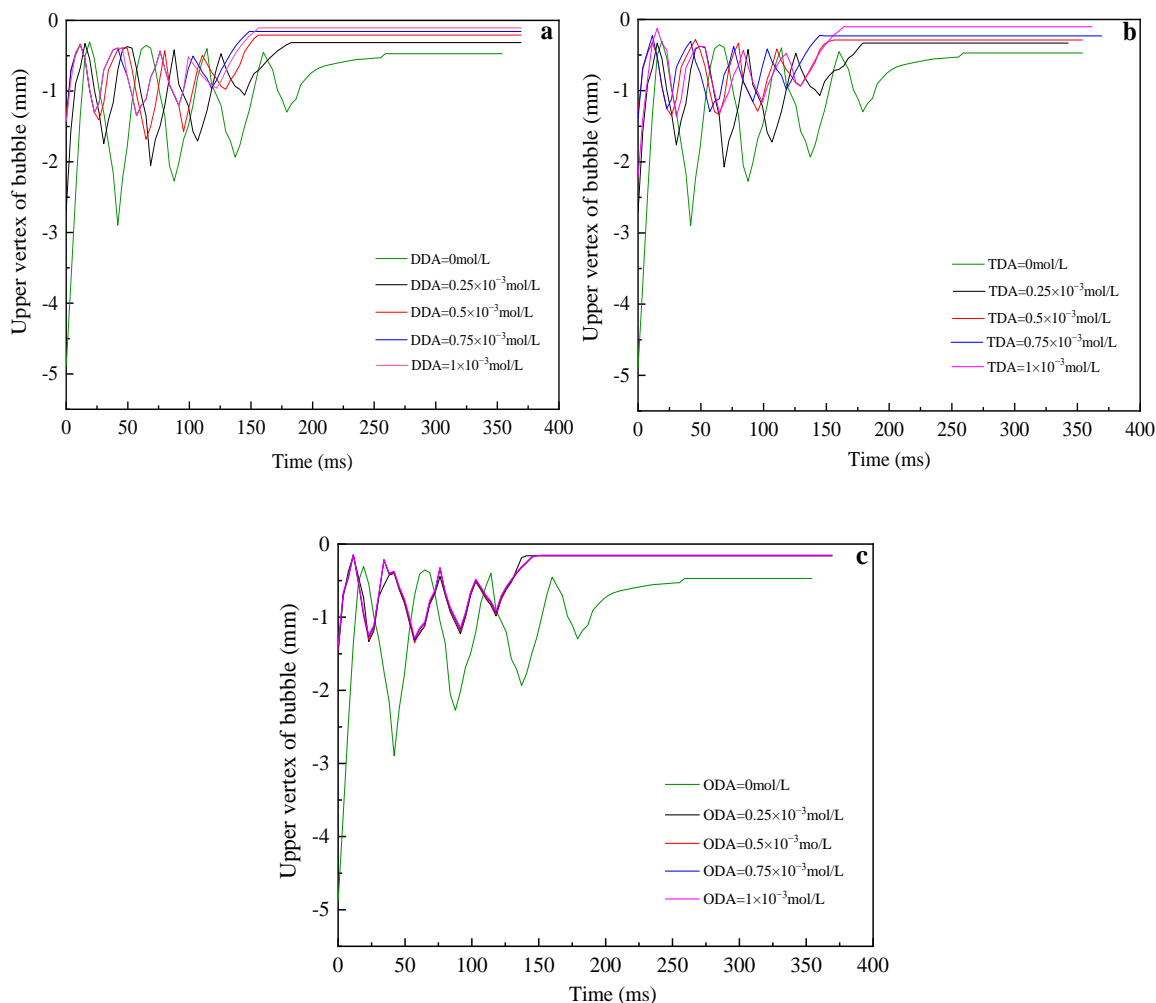
Figure 5. The rising trajectory of the bubble and its interaction under different reagent conditions. (**a**) DDA solutions. (**b**) TDA solutions. (**c**) ODA solutions.

As shown in Figure 5, the bubble is close to the quartz plate in pure water. It does not adhere to the quartz surface immediately after contact, but rebounds after deformation to the limit degree and breaks away from the quartz surface. After rebounding to a certain distance, the bubble continues to move upward. Due to energy dissipation, the bubble rises less than the first approach's speed. After four "collision-bounce" processes, the bubbles stop bouncing and stay on the solid surface. As the contact time increases, the liquid drainage process gradually reaches equilibrium, and the bubbles can stably attach to the quartz surface. The time from the first impact to when the bouncing stops is about 160 ms.

The collision and adhesion process between bubbles and quartz sheets is similar to the action process in pure water in different concentrations of long-chain amine solution. However, the time required from the beginning of impact for bubbles to stop rebounding and the maximum rebound distances are different under different reagent conditions. The induction time and steady-state liquid film thickness are also different. In general, as the concentration of the reagent solution increased, the movement speed of the bubble decreased, the maximum rebound distance decreased (about 1.5 mm), and the time from the beginning of impact to the end of rebound shortened (about 50 ms). This is because the reagent will change the state of bubble motion, the nature of the solution, and the nature of the quartz surface, and also because the rate of drainage during the interaction between the two is not the same as the thickness of the liquid film in the final steady state.

3.1.2. Bubble and Quartz Collision-Rebound Duration and Maximum Rebound Distance

In order to quantitatively analyze the interaction process between bubbles and quartz sheets, the collision-rebound duration of bubbles and quartz and the maximum rebound distance curves of bubbles were drawn under different reagent conditions, and the results are shown in Figure 6.
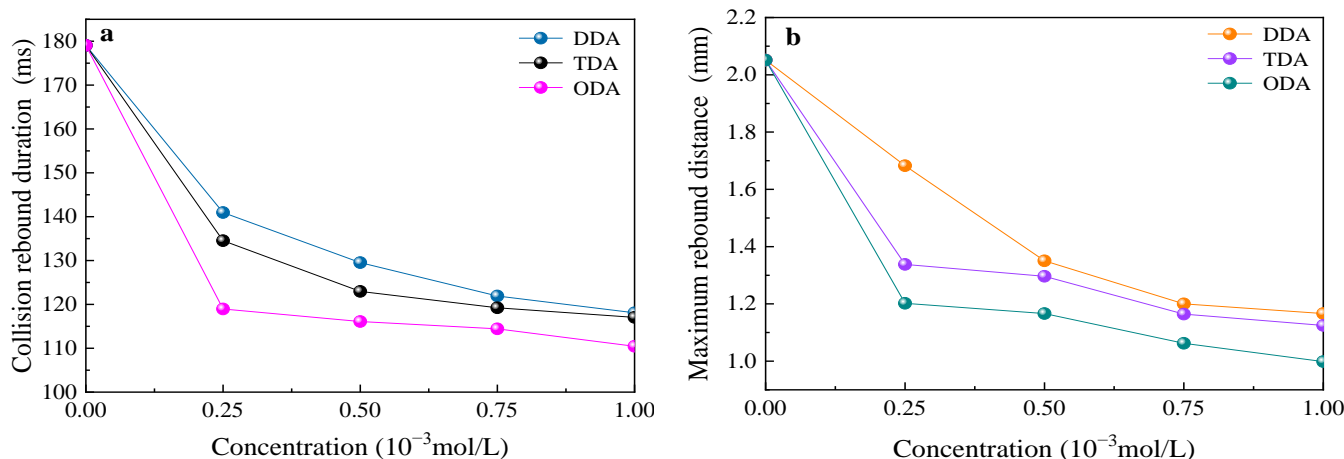
Figure 6. The collision and rebound of bubbles and quartz under different reagent conditions. (**a**) Collision-rebound duration. (**b**) The maximum rebound distance.

As shown in Figure 6, the concentration and type of the reagent impacted the collision-rebound process of the bubble. Viewed as a whole, the collision-rebound duration and the maximum rebound distance were negatively correlated with the reagent concentration and the carbon chain length of the amine molecule. At the same time, with the increase in reagent concentration, the range of the collision-rebound process duration and the maximum rebound distance decreased. This shows that there was an equilibrium trend; the longer the carbon chain length, the lower the reagent concentration reaching the equilibrium. According to Ling Xiangyang's research on foam stability [42], as the reagent concentration increases, more amines accumulate in the bottom of the bubble during the rising process, resulting in a more obvious "Marangoni" effect [43] (The Marangoni effect occurs when there is a gradient in surface tension at the interface of two phases. This phenomenon occurs mainly at gas-liquid interfaces, and as the solute concentration, surfactant concentration, and temperature along the interface change, the surface tension usually changes as well). As a result, the agents gathered at the bottom of the bubble will move towards the top of the bubble, increasing the dragging force on the bubble, hindering the fluidity of the liquid on the surface of the bubble, reducing the deformation of the bubble, and making its shape more spherical. Therefore, the speed and kinetic energy of the bubble are also reduced, and the process time requiring energy consumption is shorter.

3.1.3. The Induction Time and Steady-State Liquid Film Thickness Vary with the Concentration of the Reagent

The induction time is the time required for the liquid film thickness to decrease from the beginning to the minimum thickness. It is worth noting that in this test system, the final bubble and quartz adhesion reached a stable state, but did not break. The results of the induction time and steady-state liquid film thickness under different agent conditions are shown in Figure 7.

As shown in Figure 7 subfigure a, as the concentration of the agent increases, the induction time generally shows a shortening trend, though there is a small increase in some concentration ranges. The longer the carbon chain length, the lower the critical concentration of the induction time extension. During the contact process between bubbles and quartz, the area of the liquid film increases with the local increase of surface tension,

making the surface tension of the contact interface higher than that of the solution, resulting in a surface tension gradient. The liquid moves along the gradient direction, and the tendency of the liquid film to recover the original thickness increases as the concentration increases, resulting in an increased induction time.
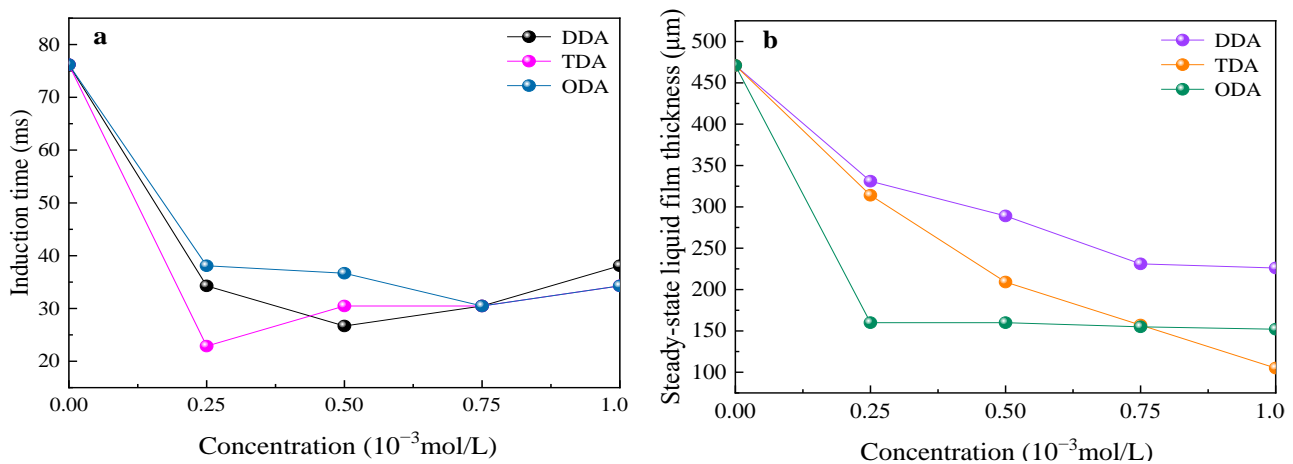
Figure 7. Induction time and steady-state liquid film thickness under different reagent conditions. (**a**) Induction time. (**b**) Steady-state liquid film thickness.

Figure 7b shows that the steady-state liquid film is significantly negatively correlated with the concentration of long-chain amines and the carbon chain lengths. At the same time, in the solution of TDA and ODA, the steady-state liquid film thickness gradually reached equilibrium with the increasing concentration of the reagent; the longer the carbon chain length, the smaller the equilibrium concentration (ODA: 0.25×10^{-3} mol/L; TDA: 0.75×10^{-3} mol/L). There was no obvious equilibrium trend in DDA solution, but the decreasing trend of the liquid film thickness slowed down gradually, indicating that the equilibrium would eventually be reached. It can be concluded that steady-state liquid film thickness is related to the type and concentration of amine collectors. When a quartz surface is treated with an amine solution before collision with a bubble, the surface unsaturated bond force is partially compensated. The higher the concentration of the reagent, the greater the compensated part, the weaker the hydration effect, and the smaller the thickness of the hydrated film [44,45].

3.2. Analysis of Phase Properties and Their Interactions Under Different Reagent Conditions

Changes in reagent conditions make the reagent molecules adsorb onto the surface of the mineral, which affects the surface properties of the mineral. At the same time, this changes the conditions for the generation of bubbles and the nature of the fluid, further affecting the size of the bubbles and their movement characteristics. In addition, changes in the conditions of the agent also alter the properties of the solution. The change in these factors comprehensively determines the result of gas-solid two-phase interactions in a flotation solution.

3.2.1. Change of Surface Tension of Solution and Surface Hydrobicity of Quartz

As surfactants, amine collectors can reduce the surface tension of the solution and, at the same time, adsorb on the surface of the mineral to enhance its surface hydrophobicity [46,47]. Changes in the surface tension and contact angle of quartz surface are detected during the experiment by means of an automatic tensiometer and contact angle measuring instrument. The solution surface tension and the contact angle of the quartz surface under different reagent conditions are shown in Figure 8.

Figure 8 shows that, viewed as a whole, the surface tension of the solution gradually decreases with the increase in the concentration of amine collectors, but the decreasing

trend gradually slows down and begins to balance. Similarly, at the same concentration, longer carbon chain lengths of the amine collector lead to a smaller surface tension in the solution. The contact angle of the quartz surface increases with the increase in concentration. However, the increasing trend also gradually slows down and eventually begins to balance as well. In addition, when the concentration of the three long-chain amines is increased to 0.75×10^{-3} mol/L, the difference in the contact angle of the quartz surface is very small. Therefore, within a certain concentration range, longer carbon chain lengths of long-chain amines result in a more obvious regulatory effect on the surface tension of the solution and the surface hydrophobicity of a solid surface, while reagent concentrations above a certain value result in a decrease in the difference between the effects of different reagents.
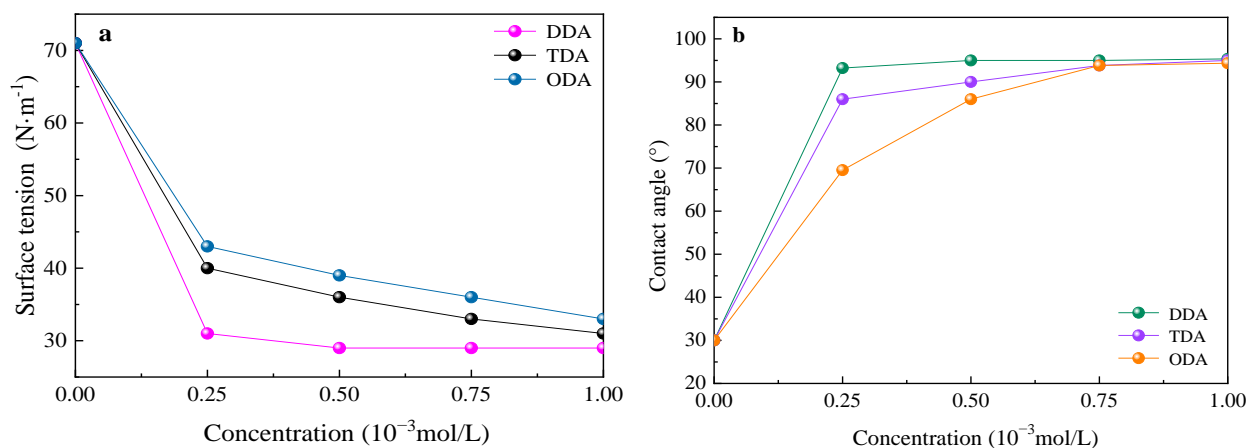

Figure 8. Surface tension of solution and contact angle of quartz surface under different reagent conditions. (**a**) Surface tension. (**b**) Contact angle.

3.2.2. Variation Characteristics of Parameters of Adsorption Process Between Reagent Molecules and Quartz

To further study the causes of the differences in the process of liquid drainage under different conditions, it is necessary to study the adsorption forms of reagents on the mineral surface and the density distribution of water molecules on the reagent-mineral surface from a microscopic perspective. The molecular dynamics of different reagent-quartz-water systems were simulated using Materials Studio 2020 software, and the adsorption energy, order degree, and density of water oxygen atoms between the amine collector and quartz were calculated, respectively. In the water environment, the adsorption energy calculation results for three amine collectors and quartz are shown in Figures 9–11.

Ignoring the influence of calculation error, the interaction energy of DDA, TDA, and ODA with the quartz surface is almost the same in the water and vacuum environments [48,49]. It can be considered that the adsorption strength of the amine collector on a quartz surface is minimally affected by the carbon chain length and can be ignored. This is because the adsorption occurs between the amine collector head group and the quartz surface under electrostatic force and has nothing to do with the non-polar group.

As shown in Figure 10, with the increase of carbon chain length, the degree of order S increases slightly; that is, compared with DDA and TDA, the ODA molecule is more perpendicular to the quartz (101) plane. When the polar group is the same, the longer the carbon chain length of the non-polar group, the closer the adsorption of reagent molecules on the quartz surface. This results in a larger angle of reagent molecules on the quartz surface, which will increase the coverage of the collector on the quartz surface and reduce its contact area with the water phase [50,51]. In addition, the length of the hydrophobic chain of the collector itself is large, which will reduce the density distribution of water molecules at a certain distance near the quartz surface, thereby increasing its hydrophobicity.
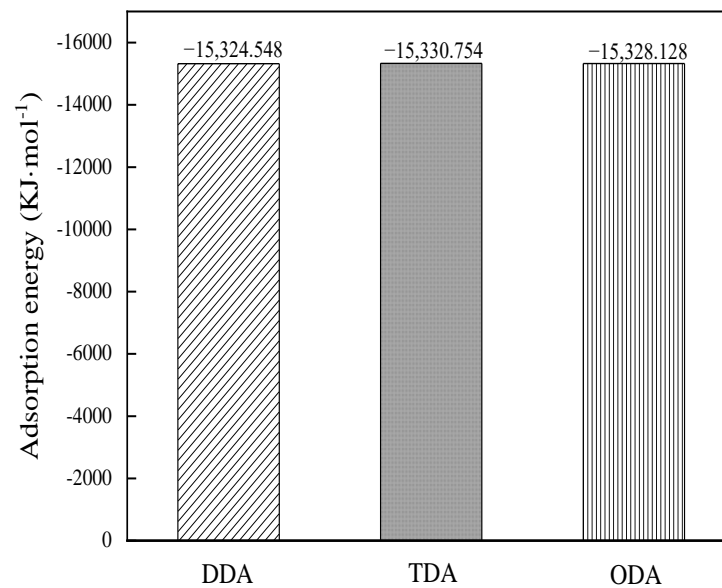
Figure 9. Adsorption energy of different cationic collectors on the quartz (101) surface.
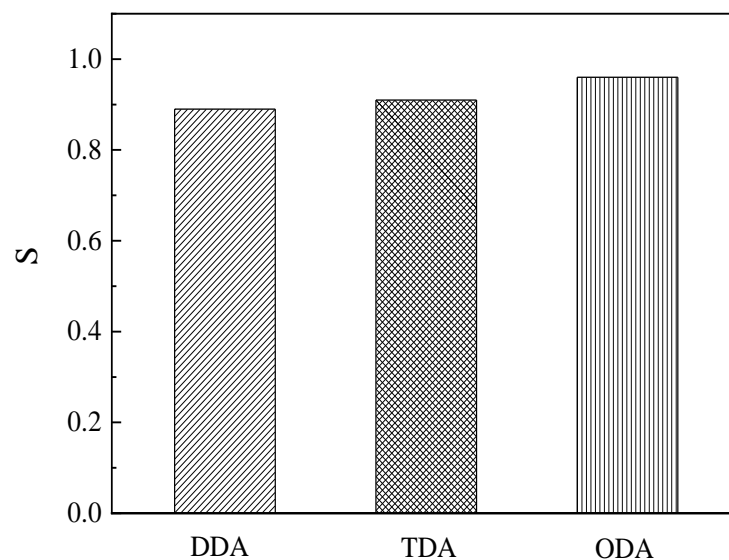
Figure 10. The influence of carbon chain length on S.

As shown in Figure 11, there are four peaks in the density of water molecules on the quartz surface after interaction with the reagent. The positions of the peaks are numerically labelled in the already graphs. With the increase in carbon chain length, the first and second peaks under the action of the three agents are very close to each other, which can be considered unrelated to the carbon chain length of the reagent. In contrast, the third and fourth peaks weaken, and the density of water molecules decreases. Macroscopically, the hydrophobicity of the quartz surface after the action of ODA is stronger, and it is easier for bubbles to adhere.

Based on the above test results, the difference in adsorption energy between primary amine collectors with different carbon chain lengths and quartz surfaces is small. However, adsorption form and water molecular density are greatly affected by the carbon chain length. Specifically, as the carbon chain length increases, the adsorption form between amine collectors and quartz surface becomes more vertical and the water molecular density decreases, with the final outcome being stronger hydrophobicity.
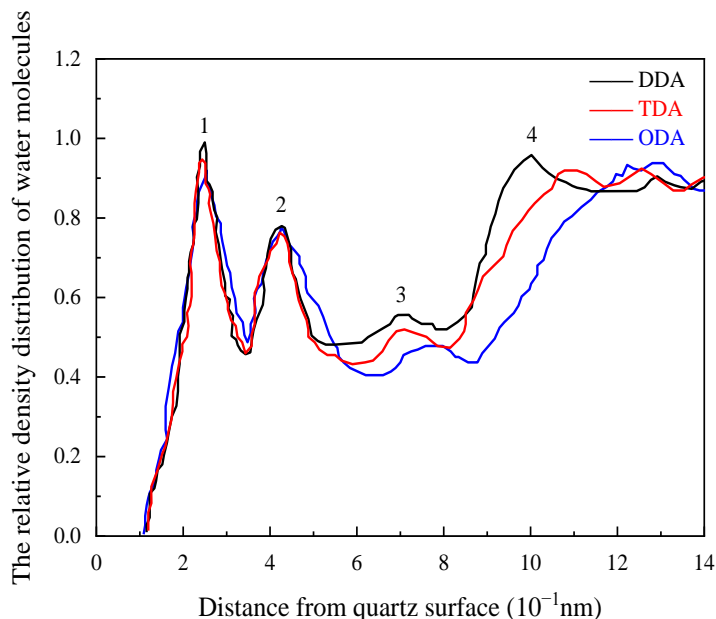
Figure 11. Relationship between the relative density distribution of water molecules and the distance from quartz surface.

3.2.3. Bubble Morphology and Movement Characteristics

Bubbles do not always remain spherical in movement and undergo varying degrees of deformation. Generally, the deformation degree of a bubble is calculated using the ratio of the maximum diameter of the bubble D_{max} to the minimum diameter D_{min} [52].

Observed by a high-speed camera system, the state of the bubble in water and 0.5×10^{-3} mol/L dodecylamine solution is shown in Figure 12.
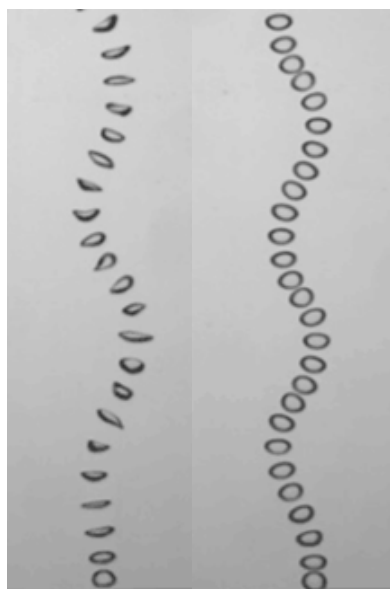

Figure 12. The motion state of bubble in water and 0.5×10^{-3} mol/L DDA solution.

After bubble generation, the bubbles showed an 'S' type rise in water and surfactant solution. However, the maximum displacement of the bubbles in the X-axis direction was different under different reagent conditions. With the increase in surfactant concentration, the maximum displacement of bubbles in the X-axis direction decreased.

In the actual flotation process, bubble deformation is often inhibited by adding surfactants, reducing the bubble movement speed [53]. To facilitate comparison, the instanta-

neous velocity and deformation degree of bubbles in pure water and DDA solution during movement were analyzed, and the results are shown in Figure 13.
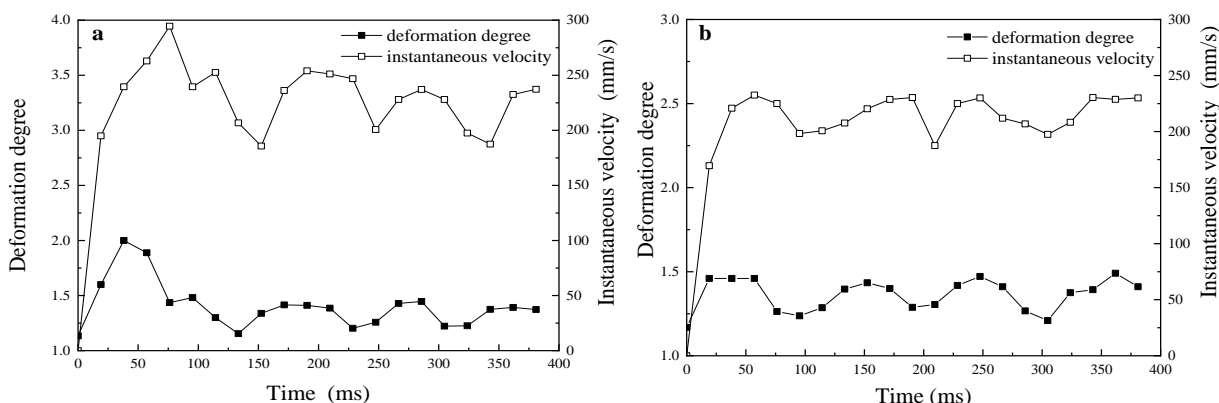
Figure 13. Relationship between the instantaneous velocity and deformation coefficient of a bubble. (**a**) Water. (**b**) 0.5×10^{-3} mol/L DDA solution.

As can be seen from Figure 13, in pure water, the bubbles first accelerate to the maximum value during the rising process and then slow down, showing periodic fluctuations around a certain value. The changing trend of bubble deformation degree is consistent with the change in velocity; when the deformation degree of the bubble is large, the speed of the bubble is high, and vice versa. In the DDA solution, the deformation degree of bubbles decreased significantly, the maximum instantaneous velocity decreased significantly, the fluctuation amplitude decreased, and the synchronization of deformation degree and velocity was higher. As amine molecules cover the bubbles during the rising process, they aggregate at the bottom of the bubbles, forming a surface tension gradient. Water molecules move along the gradient direction to prevent the bubbles from deforming, resulting in a decrease in the rising [54].

To compare the agents' actions, the average velocity curves of the bubbles in solutions of DDA, TDA, and ODA at different concentrations were drawn. The results are shown in Figure 14.
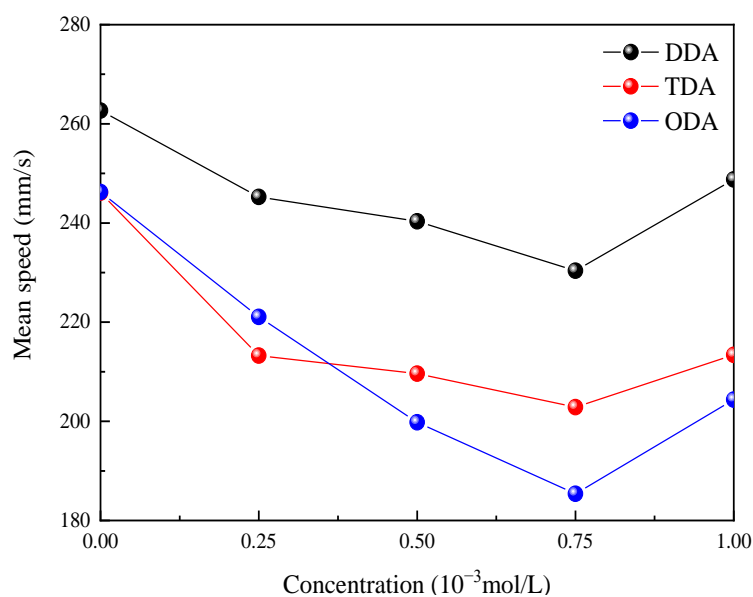
Figure 14. The influence of different concentrations of reagents on bubble rise rate.

As shown in Figure 14, in different amine solutions, the overall change trend in the average velocity of bubbles is the same; with the increase in the concentration of the agent, the average bubble velocity gradually decreases, and the decline rate also decreases continuously. All of them increase to a certain extent when the concentration is greater than 0.75×10^{-3} mol/L, indicating that there is a critical point in the regulation of the bubble rising velocity when concentrations of the agent are increased. In addition, the bubble velocity in TDA and ODA solution systems is significantly lower than that in the DDA system, and the average bubble velocity is negatively correlated with the carbon chain length. This is because the longer the carbon chain length of the long-chain amine, the smaller the deformation degree of the bubble and the smaller the rising speed [55,56]. On the other hand, when the concentration of the reagent is increased, the decrease in the surface tension and the size of the bubble will also cause a decrease in the bubble movement speed [57].

3.3. The Results of Quartz Particles Flotation Test and Their Correlation with the Parameters of Liquid Drainage Process

Flotation tests were carried out to obtain the recovery of quartz particles at different reagent concentrations, which were used to establish the correlation between the flotation results and the induction time, as well as the steady-state liquid film thickness. It has a positive effect on the prediction of flotation effectiveness.

3.3.1. Recovery of Quartz Particles at Different Reagent Concentrations

To further explore the influence of the gas–solid interaction process on the flotation effect, flotation tests were carried out on quartz particles under the same reagent conditions, and the results are shown in Figure 15.
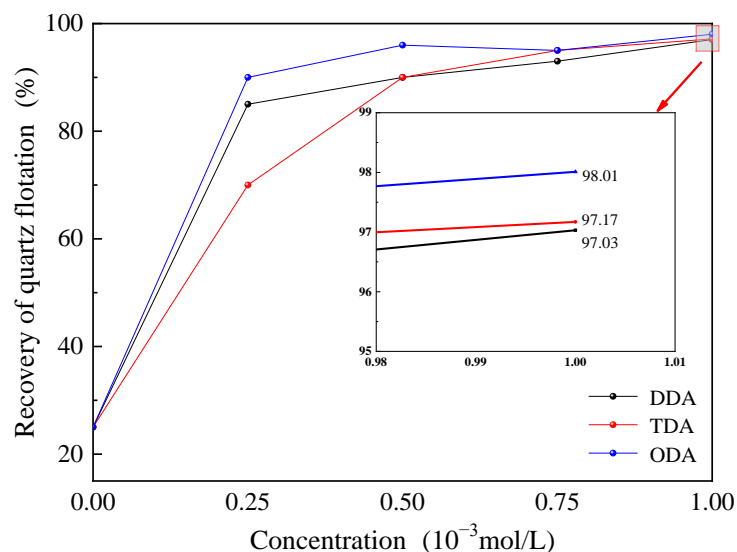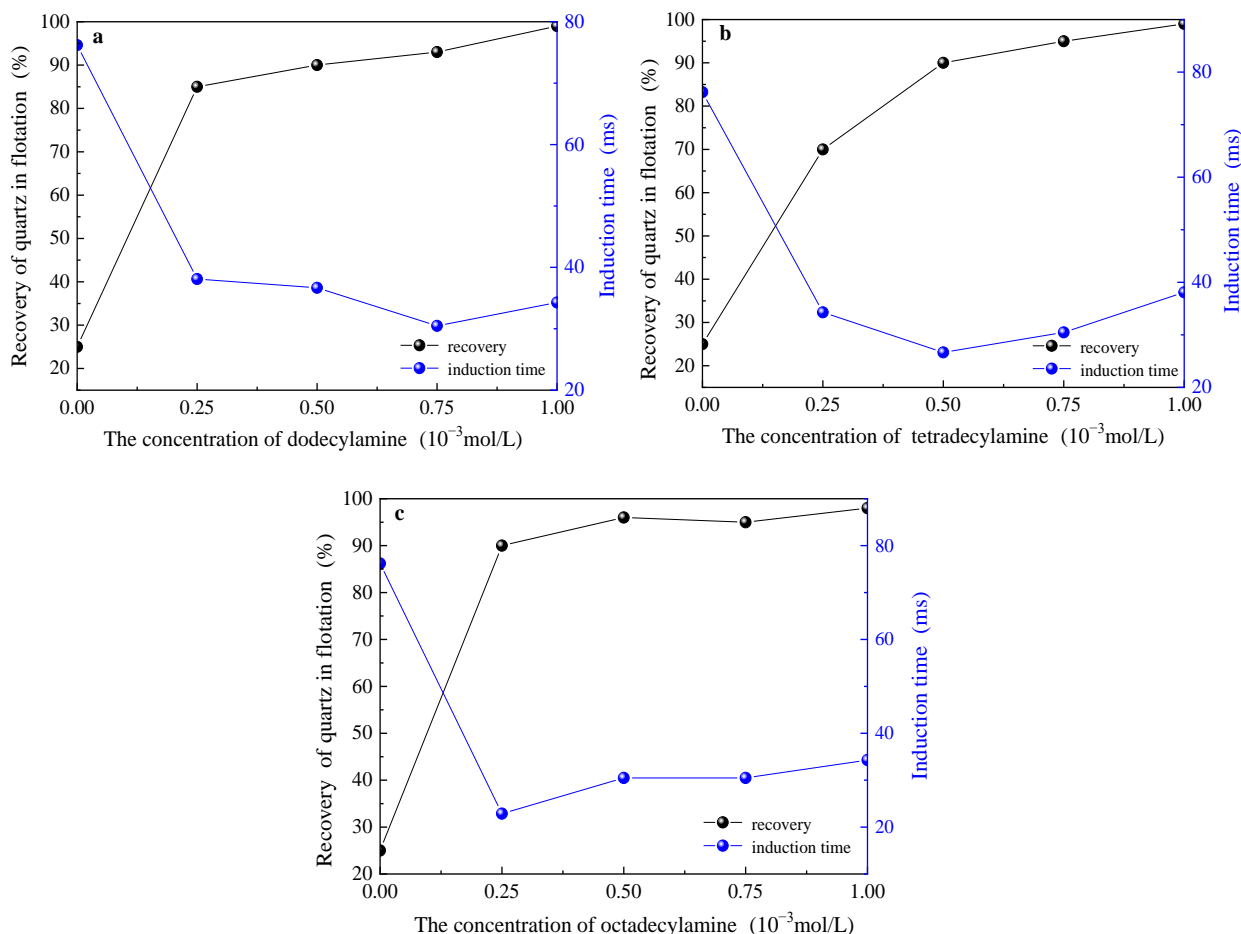

Figure 15. The recovery of quartz under different reagent conditions.

As shown in Figure 15, regardless of which amine collector is used, the recovery of quartz particles increases overall with the increase in the dosage of the agent. In the concentration range of $0–0.75 \times 10^{-3}$ mol/L, the recoveries obtained using ODA as a collector were higher than those of the other two reagent systems. When the reagent concentration was higher than 0.75×10^{-3} mol/L, the recovery difference was reduced, and all of them could reach more than 97%. In contrast, the recovery of quartz particles under the ODA system was the highest (98.01%). The results of the quartz flotation test are highly correlated with the changes in the properties and modes of action of each phase in the flotation system.

3.3.2. Correlation Between Induction Time and Quartz Particles Recovery

Induction time is essential in the interaction between flotation bubbles and minerals. Figure 16 shows the corresponding relationship between induction time and recovery under the conditions of DDA, TDA, and ODA with different concentrations obtained by combining the shooting results of high-speed dynamic cameras and flotation tests.
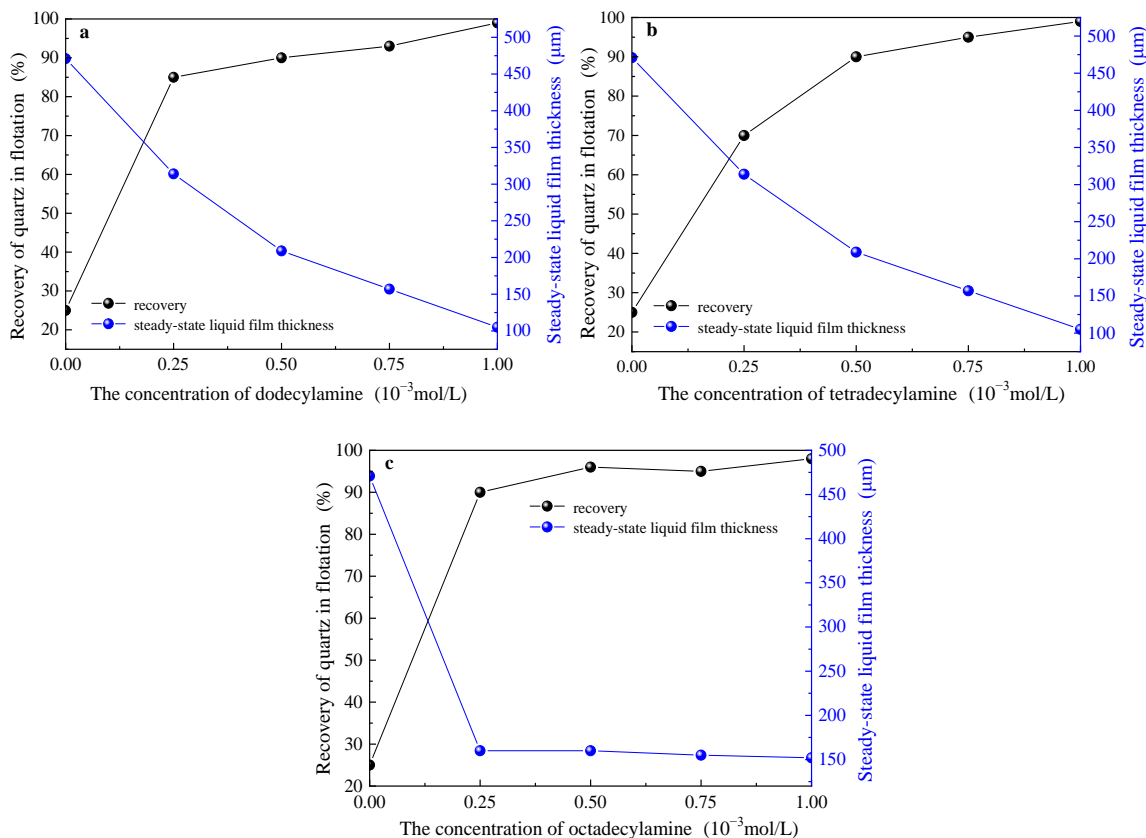

Figure 16. Comprehensive effect of reagent concentration on induction time and recovery of quartz particles. (**a**) DDA. (**b**) TDA. (**c**) ODA.

Figure 16 shows that, under different concentrations of three different agents, the recovery of quartz flotation is negatively correlated with the induction time; that is, the shorter the induction time, the higher the recovery. However, when the induction time is reduced to a certain extent, it is no longer related to the recovery. The process of liquid drainage is the speed control step of flotation. When the induction time is extended, the number of particles that can successfully adhere to the bubble is small, reducing the productivity. When the induction time is reduced to a certain extent, there is little difference in the number of adhesions between particles and bubbles, and the main factor affecting the flotation effect changes the stability of adhesion between gas and solid. Therefore, when the concentration of the reagent increases to a certain extent, the induction time becomes longer due to the significant Marangoni effect. However, the adhesion between the gas-solid phase is more stable due to the enhanced hydrophobicity of the quartz surface, and the flotation recovery increases rather than decreases.

3.3.3. Correlation Between Steady-State Liquid Film Thickness and Quartz Particles Recovery

The relationship between steady-state liquid film thickness and flotation recovery of quartz in DDA, TDA, and ODA systems is shown in Figure 17.

Figure 17. Comprehensive effect of reagent concentration on steady-state liquid film thickness and recovery of quartz particles. (**a**) DDA. (**b**) TDA. (**c**) ODA.

As shown in Figure 17, in the three reagent systems, the steady-state liquid film thickness is consistent with the rule of induction time. It is also negatively correlated with the flotation recovery of quartz in general; the thinner the liquid film thickness between bubbles and minerals, the higher the flotation recovery. This shows that the liquid film thickness during the interaction between bubbles and mineral particles can characterize adhesion stability. A thinner hydration film makes the adhesion process more stable, makes it more difficult for mineral particles to detach from the bubble, and improves the flotation effect. The results show that the thickness of the liquid film and the induction time can be key indexes to predict the flotation effect and have important reference values to accurately predict the flotation effect. In contrast, the steady-state liquid film thickness, which is not affected by the Marangoni effect, has higher accuracy in the characterization of the surface interaction between bubbles and solid particles to a certain extent.

4. Conclusions

In the present work, we systemically investigated the parameters variation in the dynamic interaction process between rising bubbles and quartz in long-chain amine solutions at the same concentration as the actual flotation process. We focused on clarifying the relevance of these parameters and identifying the drainage process parameters that can accurately predict the flotation results. The variation trend of the steady-state liquid film thickness is found to have the strongest correlation with the recovery of quartz by flotation.

(1) The collision and rebound process between the bubbles and the quartz plates in the long-chain amine solution is similar to that in pure water, and it takes four rebounds to stay on the surface of the quartz plate and to start the liquid drainage process. The duration of the collision-rebound process and the maximum rebound distance were negatively correlated with the concentration of the reagent and the carbon chain length, and there was an equilibrium trend.

(2) The induction time decreases with the increase in reagent concentration. Finally, there is still a hydration film between the bubble and the surface of the quartz plate. The stable-state liquid film thickness has a significant negative correlation with the concentration of long-chain amine and the carbon chain length; the longer the carbon chain length, the lower the adhesion equilibrium concentration.

(3) With the increase in the concentration of long-chain amine, the surface tension of the solution decreases, and the hydrophobicity of quartz increases. The longer the carbon chain length, the more obvious the regulatory effect. The effect difference of different agents decreases with the increase of the concentration of agents. At the microscopic level, the adsorption form of the amine collector and quartz surface becomes more vertical as the carbon chain length increases. The water molecular density also becomes smaller and eventually shows stronger hydrophobicity.

(4) Compared with pure water, the deformation degree of the bubble in dodecylamine solution is significantly reduced, and the deformation degree and velocity synchronization are higher. The average velocity of bubbles decreases with the increase in the concentration, and there is a critical point of control. The bubble velocity of tetradecylamine and octadecylamine solutions was significantly lower than that of the dodecylamine system.

(5) When octadecylamine is used as a collector, the recovery of quartz particles is higher than that of the other two reagent systems. The results of flotation tests are highly correlated with the changes in phase properties and modes of action in the flotation system. In contrast, the steady-state liquid film thickness can more accurately characterize the interaction between bubbles and particle surfaces to some extent.

References

1. Liu, H.S.; Yang, C.H.; Wang, Y.L.; Gui, W.H. Analysis of bubble size and parameter optimization in microbubble flotation. *Miner. Eng. Res.* **2009**, *24*, 58–61.
2. Shen, Z.C.; Lu, S.J.; Shi, S.X.; Chen, D.; Yang, L.J. Analysis and discussion of characteristic parameters of bubbles in KYF flotation machine-flow field measurement and simulation research on KYF flotation machine. *Nonferrous Met. Miner. Process. Sect.* **2013**, *5*, 44–49.
3. Ren, L.Y.; Xiao, D.D.; Qin, W.Q. Review on flotation of fine minerals: Increasing apparent particle size and decreasing bubble diameter. *Miner. Prot. Util.* **2024**, *44*, 1–15.
4. Cheng, Y.; Min, F.; Li, H.; Chen, J.; Fu, X.H. Effect of reagent interaction on froth stability of coal flotation. *Fuel* **2022**, *318*, 123417. [CrossRef]
5. Ceylan, A.; Aydın, Ş.B.; Göktepe, F.; Bulut, G. Relation of bubble size, grade and recovery in the copper flotation systems. *Colloids Surf. A Physicochem. Eng. Asp.* **2024**, *692*, 133929. [CrossRef]

6. Chen, Q.Y.; Zhang, J.S.; Wang, D.Z. Recent progress in the study of interaction between bubbles and particles. *Met. Ore Dress. Abroad* **2001**, *2*, 17–19.
7. Yang, S.J.; Liu, Q.X.; Ren, S.L. Research progress of bubble-particle interaction behavior in mineral flotation. *Nonferrous Met. (Miner. Process. Sect.)* **2024**, *1*, 18–27.
8. Wang, S.W.; Wang, Y.H.; Kong, R.J. Investigation of flotation bubble-particle attachment interactions influenced by monovalent cations and cationic surfactants from macro and molecular scales. *Adv. Powder Technol.* **2024**, *35*, 104549. [CrossRef]
9. Zhao, Z.G. *Chemical Base for Interphase*; Chemical Industry Press: Beijing, China, 1996.
10. Cui, G.W. *Surface and Interphase*; Tsinghua University Press: Beijing, China, 1990.
11. Petra, W.; Borje, N.; Peter, R. Risk assessment of false-positive quantitative real-time PCR results in food, due to detection of DNA or iginating from dead cells. *J. Microbiol. Methods* **2005**, *60*, 315–323.
12. Yoon, R.H. The role of hydrodynamic and surface forces in bubble-particle interaction. *Int. J. Miner. Process.* **2000**, *58*, 129–143. [CrossRef]
13. Zhang, X.Y.; Ren, L.Y.; Bao, S.X.; Zhang, Y.M.; Chen, G.H.; Chen, B. Insight into the Effect of Nanobubbles on Fine Muscovite Powder Flotation in Different Dodecylamine Concentrations and Stirring Intensities: Kinetics and Mechanism. *Minerals* **2024**, *14*, 694. [CrossRef]
14. Finch, J.A.; Dobby, G.S. *Column Flotation*; Pergamon Press: Oxford, UK, 1990.
15. Schulze, H.J. Physico-chemical elementary processes in flotation. *Dev. Miner. Process.* **1983**, *4*, 320.
16. Hu, H.S. *Study on Mineralization Process Characteristics of Low-Rank Coal-Gas/Oil Bubbles and Strengthening of Flotation Process of Active Oil Bubbles*; China University of Mining and Technology: Beijing, China, 2020.
17. Chen, S.X. *Surface/Interface Characteristics of Shendong Long Flame Coal and Its Adhesion Mechanism to Active Oil Bubble*; China University of Mining and Technology: Beijing, China, 2020.
18. Ren, L.Y.; Zhang, Y.M.; Qin, W.Q.; Bao, S.X.; Wang, P.P.; Yang, C.R. Investigation of condition-induced bubble size and distribution in electroflotation using a high-speed camera. *Int. J. Min. Sci. Technol.* **2014**, *24*, 7–12. [CrossRef]
19. Wang, Y.L.; Liu, Q.S.; He, Q.; Ding, S.H.; Shi, W.Q.; Gui, X.H.; Xing, Y.W. Collision-induced detachment behavior of bubble-particle aggregate at air-water interface. *Powder Technol.* **2024**, *446*, 120189. [CrossRef]
20. Yang, J.J.; Yao, J.J.; Li, Y.P. Visualization of bubble impact on solid surface in flotation process. *Water Treat. Inf. Rep.* **2014**, *6*, 14–18.
21. Zhang, S.J. *Study on Collision and Adsorption Law of Particles and Bubbles in Slime Flotation Process*; China University of Mining and Technology: Beijing, China, 2015.
22. Li, G.S.; Han, J.Z.; Deng, L.J.; Cao, Y.J.; Ran, J.C.; Wang, J.C. Collision and adhesion process of bubbles on coalsurface. *J. China Coal Soc.* **2016**, *41*, 2841–2846.
23. Krasowska, M.; Malysa, K. Kinetics of bubble collision and attachment to hydrophobic solids: I. Effect of surface roughness. *Int. J. Miner. Process.* **2007**, *81*, 205–216. [CrossRef]
24. Zhao, Z.F.; Li, Y.Z.; Zhang, Z.J. Effect of surfactant on the attachment between coal particles and bubbles: An experimental and molecular dynamics simulation study. *Fuel* **2023**, *337*, 127272. [CrossRef]
25. Nguyen, A.V.; Ralston, J.; Schulze, H.J. On modelling of bubble-particle attachment probability in flotation. *Miner. Process.* **1998**, *53*, 225–249. [CrossRef]
26. Wang, X.X.; Yu, M.; Wang, Y.M.; Ma, C.; Bu, X.N. Research progress of flotation separation and strengthening methods of fine slime. *Clean Coal Technol.* **2024**, *30*, 185–202.
27. Levie, M.; Park, H.S.; Kang, S.; Kim, H. Separation of chalcopyrite from a siliceous copper ore using polyethylene oxide as a depressant: An experimental study complimented by theoretical investigation. *Miner. Eng.* **2023**, *204*, 108445. [CrossRef]
28. Luo, X.M.; Sun, C.Y.; Yin, W.Z. Application status of Atomic force microscopy in Mineral processing. *Min. Mach.* **2011**, *39*, 80–85.
29. Guo, Y.; Ren, S.L. Application status of Atomic Force microscopy technology in mineral flotation. *Non-Ferr. Met. (Miner. Process. Part)* **2022**, *01*, 73–79.
30. Wang, X.M.; Lu, Y. New progress of surface analysis technology and its application in mineral engineering research: Atomic Force microscopy. *J. Guizhou Univ. (Nat. Sci. Ed.)* **2018**, *35*, 1–12.
31. Yu, J.; Mei, T.G.; Chen, W.; Liu, S.; Liu, G.Y. Understanding the sequential flotation separation of fluorite, barite and calcite through the AFM adhesion force. *Chem. Eng. Sci.* **2024**, *285*, 119608. [CrossRef]
32. Shitian, S.Z.; Dong, X.H.; Yu, T. Direct determination of the interaction force between fine particlesand bubbles in surfactant aqueous solution. *Foreign Met. Ore Process.* **2005**, *7*, 38–43.
33. Zhu, C.Y.; Yu, F.; Li, M.; Sun, L.J.; Xing, Y.W.; Gui, X.H. Study on the adhesion mechanism of bubbles to coal surface based on different hydrophobic coal models. *Coal Prep. Technol.* **2024**, *52*, 30–36.
34. Zhang, F.F.; Cao, Y.J.; Xing, Y.W.; Gui, X.H.; Sun, L.J.; Yang, H.C.; Li, M. Experimental study on Bubble interaction behavior of flotation particles at micro/Nano scale. *J. China Coal Soc.* **2022**, *47*, 276–284.
35. Xing, Y.W.; Gui, X.H.; Han, H.S.; Sun, W.; Cao, Y.J.; Liu, J.T. Bubble-particle attachment science-study on hydrophobic force be-tween bubble and particle based on AFM and DWFA. *J. China Coal Soc.* **2019**, *44*, 1580–1585.
36. Israelachvili, J.N.; Wennerström, H. Role of hydration and water structure in biological and colloidal interactions. *Nature* **1996**, *379*, 219–225. [CrossRef]
37. Peng, D.Q. *Research on Behavior Characteristics and Control Intelligence of flotation Bubbles Based on Image Processing*; Taiyuan University of Technology: Taiyuan, China, 2023.

38. Li, D.L.; Zhang, J.Y.; Wang, W.Z.; Han, J.K.; Li, F.J. Research Progress of Bubble Movement Characteristics in Flotation System. *Nonferrous Met. (Miner. Process.)* **2024**, 49–58.

39. Xie, H.J.; Nie, D.P. Effect of Quartz on the Stability of Flotation Foam and Its Mechanism. *Nonferrous Met. (Miner. Process.)* **2024**, 40–47.

40. Zhang, J.X.; Liu, F.; Niu, F.S.; Chen, Y.Y. Research on Flotation Separation of Fine-grained Hematite/Quartz Based on Asynchronous Agglomeration Regulation. *Nonferrous Met. Eng.* **2024**, *14*, 116–122.

41. Zhang, X.R.; Xie, Y.; Shang, Y.B.; Zhu, Y.G.; Xiong, W.; Lu, L. Application of Organic Macromolecular Depressants with Polycarboxylic Groups in Reverse Flotation of Hematite Ore for Removal of Silicate. *Nonferrous Met. (Miner. Process.)* **2022**, 164–170+176.

42. Ling, X.Y. *Study on the Mechanism of Foam Stability and Particle Motion at the Gas-Liquid Interface on Froth Phase Flotation*; China University of Mining and Technology: Beijing, China, 2019.

43. Scriven, L.E.; Sternling, C.V. The Marangoni Effects. *Nature* **1960**, *187*, 186–188. [CrossRef]

44. Xing, Y.W. *Research on Particle Bubble Interaction and Liquid Film Thinning Kinetics*; China University of Mining and Technology: Beijing, China, 2018.

45. Xu, M.D. *Process and Kinetics of Flotation Two-Phase Foam Drainage*; China University of Mining and Technology: Beijing, China, 2020.

46. Li, K.Q.; Sun, H.R.; Huang, R.W.; Wang, Y.L.; Yuan, Z.G.; Su, D.S. Effect of Amine Collectors with Different Structures on the Separation of Magnesite from Quartz. *Met. Mine* **2023**, 123–131.

47. Luo, X.M.; Wu, X.T.; Qi, L.P.; Wei, D.Y.; Li, C.; Yang, W.; Wang, Y.F. Foam Stability of Two Phase and Hematite/Quartz Three Phase in Four Amine Collector Systems. *Nonferrous Met. Eng.* **2022**, *12*, 84–90.

48. Yan, Y.W.; Luo, H.H.; Zhao, J.; Liu, Y.T.; Zhang, Z.Y. Application status and development prospect of amine collectors. *Miner. Conserv. Util.* **2022**, *42*, 59–66.

49. Wang, B.Y.; Xu, X.Y.; Duan, H.; Chen, X. Quantitative structure-activity relationship of amine collector adsorption on quartz surface. *J. Northeast. Univ. (Nat. Sci.)* **2020**, *41*, 131–136.

50. Liu, Z.H. *Study on the Interfacial Interaction Mechanism Between Hydrocarbon Oil-Carboxylic Acid Composite Collector and Low Rank Coal*; China University of Mining and Technology: Beijing, China, 2022.

51. Zhang, C.F.; Yu, Q.Y.; Cao, Y.J.; Fan, G.X. Research progress of flotation reagents and Surface Modification of ilmenite. *Chin. J. Nonferrous Met.* **2021**, *31*, 3675–3689.

52. Wang, G.H. *Research on Bubble Movement Behavior in Confined Flow Channel Driven by Negative Pressure*; Zhengzhou University of Light Industry: Zhengzhou, China, 2024.

53. Pang, S.H. Study on the effect of foaming agent on the characteristics of flotation bubbles. *Coal Prep. Technol.* **2024**, *52*, 44–50.

54. Wu, Y.; Tang, M.; Niu, X.Y.; Fu, J.H.; Luo, J.X. Effect of ζ potential on the flotation behavior of serpentine in xanthate/black powder system. *Compr. Util. Miner. Resour.* **2024**, 1–12.

55. Wang, J.C.; Li, G.S.; Han, J.Z.; Liu, C.Q. Study on the influence of foaming agent on bubble shape and velocity in solution. *Coal Eng.* **2016**, *48*, 142–145.

56. Liu, Y.Y. *Experimental Study on the Effect of Surfactants on the Dynamic Characteristics of Flotation Bubbles*; Chang'an University: Xi'an, China, 2011.

57. Malysa, K.; Krasowska, M.; Krzan, M. Influence of surface active substances on bubble motion and collision with various interfaces. *Adv. Colloid Interface Sci.* **2005**, *114–115*, 205–225. [CrossRef]